

# Effect of cosmic ray/X-ray ionization on supermassive black hole formation

Kohei Inayoshi<sup>1\*</sup> and Kazuyuki Omukai<sup>1</sup> †

<sup>1</sup>*Department of Physics, Kyoto University, Kyoto 606-8502, Japan*

## ABSTRACT

We study effects of external ionization by cosmic rays (CRs) and X-rays on the thermal evolution of primordial clouds under strong far-ultraviolet (FUV) radiation. A strong FUV radiation field photodissociates  $\text{H}_2$  and quenches its cooling. Even in such an environment, a massive cloud with the virial temperature  $\gtrsim 10^4$  K can contract isothermally at 8000 K by the hydrogen Lyman  $\alpha$  cooling. This cloud collapses monolithically without fragmentation, and a supermassive star ( $\gtrsim 10^5 M_\odot$ ) is believed to form at the center, which eventually evolves to a supermassive black hole (SMBH). However, candidates of FUV sources, including star-forming galaxies, are probably sources of strong CRs and X-rays, as well. We find that the external ionization promotes  $\text{H}_2$  production and elevates the threshold FUV intensity  $J_{\text{crit}}$  needed for the SMBH formation for CR energy density  $U_{\text{CR}} \gtrsim 10^{-14}$  erg cm<sup>-3</sup> or X-ray intensity  $J_X \gtrsim 10^{-24}$  erg s<sup>-1</sup> cm<sup>-2</sup> sr<sup>-1</sup> Hz<sup>-1</sup> at 1 keV. The critical FUV flux increases as  $J_{\text{crit}} \propto U_{\text{CR}}^{1/2}$  ( $\propto J_X^{1/2}$ ) in the high CR (X-ray, respectively) limit. With the same value of FUV intensity at the Lyman limit (13.6 eV), the  $\text{H}^-$  photodissociation rate, with threshold of 0.755 eV, increases and the  $\text{H}_2$  abundance decreases with decreasing effective temperature of the FUV sources  $T_*$ . The lower value of  $T_*$  thus results in the lower critical FUV flux  $J_{\text{crit}}$  at the Lyman limit. Using an empirical relation between intensities of FUV and CRs/X-rays from nearby star-forming galaxies, we find that external ionization effect remarkably enhances the critical FUV flux for sources with  $T_*$  as high as  $10^5$  K and composed of stars with  $\lesssim 100 M_\odot$  to a level that is not realized in any halo. This indicates that, to induce SMBH formation, the FUV sources must be either Pop II/I galaxies with low brightness temperature ( $T_* \sim 10^4$  K), Pop III galaxies ( $T_* \sim 10^5$  K) with a very top-heavy IMF, or Pop III galaxies too young to harbor sources of CRs/X-rays, for example, supernova remnants or high-mass X-ray binaries.

**Key words:** stars: formation — stars: Population III — dark ages, reionization, first stars

## 1 INTRODUCTION

The origin of supermassive black holes (SMBHs), ubiquitously existing at the centers of present-day galaxies, still remains a mystery. Among them, the existence of the luminous SDSS quasars with estimated SMBH masses of a few times  $10^9 M_\odot$  by their luminosities  $\gtrsim 10^{47}$  erg s<sup>-1</sup> at redshift  $z \gtrsim 6$ , when the age of Universe is less than 1 Gyr, (e.g., Fan 2006) poses serious constraints on their formation and evolution scenarios. Several authors have studied models for the SMBH growth by merger and gas accretion (e.g., Haiman & Loeb 2001; Volonteri, Haardt & Madau 2003; Li et al. 2007), starting from stellar-mass black holes (BHs),

which are remnants of first generation of stars. However, various negative feedbacks prohibit their rapid growth.

In a merger event, the BH experiences strong recoil, with typical velocity  $\gtrsim 100$  km s<sup>-1</sup>, owing to gravitational wave emission (Herrmann et al. 2007; Koppitz et al. 2007). The recoil velocity depends on the spin configuration of the merging pair and can reach as high as  $\sim 4000$  km s<sup>-1</sup> for the anti-parallel spins (Campanelli et al. 2007). In high-redshift universe, typical halos tend to be low-mass and their escape velocity ( $\lesssim 10$  km s<sup>-1</sup>) is smaller than the recoil velocity. If BHs are ejected from their host halos in merging events, the BH growth process must repeat again from scratch. On the other hand, in the gas-accretion scenario, the accretion rate onto the BH is at most similar to the Eddington limit. In this case, it takes  $\sim 1$  Gyr to form a SMBH with  $10^9 M_\odot$  from a BH with  $100 M_\odot$ . Although this is marginally consistent

\* E-mail: inayoshi@tap.sphys.kyoto-u.ac.jp

† E-mail: omukai@tap.sphys.kyoto-u.ac.jp

with the existence of SMBHs at  $z \gtrsim 6$ , this requires constant supply of gas at the Eddington rate. However, recent hydrodynamical simulations demonstrate that radiative feedback from the accreting black hole prevents such efficient accretion (Milosavljević, Couch & Bromm 2009; Alvarez, Wise & Abel 2009).

We here explore another possibility that the seed BHs form via gravitational collapse of supermassive stars (SMSs) and thus are as massive as  $\gtrsim 10^5 M_\odot$  from the beginning. Evolution and general relativistic instability of the supermassive stars have been investigated by many authors (e.g., Chandrasekhar 1964a, b; Zeldovich & Novikov 1971; Shapiro & Teukolsky 1983). Among them, Shibata & Shapiro (2002) calculated the collapse of a rotating supermassive star into a SMBH and found that most of the mass originally in the SMS is eventually locked in the BH ( $M_{\text{BH}} \simeq 0.9 M_{\text{SMS}}$ ).

The biggest challenge in this scenario is how such supermassive stars are formed. A promising pathway is through the collapse of a cloud in a halo under an extremely strong far-ultraviolet (FUV) radiation field. The FUV radiation in the Lyman and Werner bands (11.2–13.6 eV) dissociates  $\text{H}_2$  molecules, which are important coolants in a primordial gas in the low-temperature ( $\lesssim 8000$  K) regime. Under a FUV radiation field exceeding a critical value,  $J_{\text{crit}} \simeq 300$  ( $10^5$ ) in the unit of  $10^{-21} \text{ erg s}^{-1} \text{ cm}^{-2} \text{ sr}^{-1} \text{ Hz}^{-1}$ , for the stellar-type radiation with brightness temperature  $T_* = 10^4$  K ( $10^5$  K, respectively), the  $\text{H}_2$  formation is suppressed all the way during the protostellar collapse and then its cooling is totally quenched (Omukai 2001; Shang, Bryan & Haiman 2010). In this case, the collapse proceeds almost isothermally at  $\simeq 8000$  K by hydrogen Lyman  $\alpha$  and two-photon emission, and  $\text{H}^-$  bound-free emission. Unlike the case with weaker radiation field, where the  $\text{H}_2$  line cooling induces fragmentation to clumps of  $\sim 10^3 M_\odot$ , such a cloud eludes fragmentation and collapses directly to a supermassive star of  $\gtrsim 10^5 M_\odot$  (Bromm & Loeb 2003; Regan & Haehnelt 2009a, b), and collapses eventually into the seed BH for the subsequent growth to a SMBH.

The critical FUV flux for the suppression of the  $\text{H}_2$  cooling is far above the expected mean value of the background radiation. Studying the spatial correlation between halos, Dijkstra et al. (2008) derived the probability distribution of the intensity of Lyman-Werner flux  $J_{21}^{\text{LW}}$  (in units of  $10^{-21} \text{ erg s}^{-1} \text{ cm}^{-2} \text{ sr}^{-1} \text{ Hz}^{-1}$ ) incident on halos with mass  $\sim 10^8 M_\odot$  collapsing at redshift  $z \simeq 10$ . The estimated mean Lyman-Werner background is  $J_{21}^{\text{LW}} = 40$ , far below the critical value. This means that such intense FUV fields are only realized in neighborhoods of strong FUV sources. They also estimated the fraction of halos bathed in radiation fields exceeding the threshold value  $J_{\text{crit}}$ . This fraction is  $10^{-6}$  for  $J_{\text{crit}} = 10^3$  and decreases exponentially with increasing  $J_{\text{crit}}$  ( $\gtrsim 2 \times 10^3$ ). A small difference in  $J_{\text{crit}}$  significantly affects the number of halos bearing supermassive stars, and thus correct knowledge of the critical FUV flux is crucial in estimating the number of seed BHs.

So far, the critical FUV flux  $J_{\text{crit}}$  has been studied only in cases where the incident radiation consists of components below the Lyman limit (Omukai 2001; Bromm & Loeb 2003; Shang et al. 2010). However, strong FUV sources, i.e., actively star-forming galaxies, are expected to contain a large number of massive stars and possibly some mini-quasars. Since massive stars end their lives as supernovae and leave

the remnants, where cosmic rays (CRs) are accelerated and X-ray photons are produced, sources of strong FUV radiation can also be those of CRs and X-ray photons. Similarly, mini-quasars and high-mass X-ray binaries emit soft X-ray radiation. The incident flux is thus expected to have such high-energy components. If present, CRs and X-rays enhance the ionization degree of gas and increase the amount of  $\text{H}_2$ , which is formed by electron-catalysed reactions. In fact, Haiman, Rees, & Loeb (1996) and Glover & Brand (2003), who studied the condition for virialized minihalos under both FUV and X-ray irradiation to be able to cool via  $\text{H}_2$  line emission, found that the FUV photodissociation effect is somewhat alleviated by the X-ray ionization.

In this paper, we consider similar effects of X-ray and CR ionization on more massive halos with the virial temperature  $\gtrsim 10^4$  K. Even without  $\text{H}_2$  cooling, the clouds in such halos start collapsing via H atomic cooling. If the FUV field is below some critical value  $J_{\text{crit}}$ , however, abundant  $\text{H}_2$  molecules form and fragmentation of the clouds occurs at some high density during the collapse by the  $\text{H}_2$  cooling. With the enhanced  $\text{H}_2$  fraction by X-ray and CR ionization, the more FUV flux is necessary to quench its cooling, thereby boosting the critical value  $J_{\text{crit}}$ . This results in fewer number of seed BHs since the isothermal collapse via atomic cooling is required to form SMSs. Our aim is to see the dependence of the critical FUV flux  $J_{\text{crit}}$  on the amount of CRs as well as X-rays. By this way, we try to discuss the nature of the FUV sources needed to induce SMS formation.

The organization of this paper is as follows. In Section 2, we explain our model of calculation, including chemical reactions and effects of FUV, CRs/X-rays. We present our results for the evolution of the clouds irradiated by FUV radiation and ionized by CRs/X-rays in Section 3, and give analytic interpretation for the obtained critical FUV flux in Section 4. In Section 5, we use an empirical relation between intensities of FUV and CRs/X-rays from nearby star-forming galaxies and speculate conditions to induce the supermassive star formation. Finally, we summarize this paper and give some discussions in Section 6.

## 2 MODEL

### 2.1 thermal evolution

We consider thermal evolution of a metal-free cloud in a moderately massive halo with virial temperature  $\gtrsim 10^4$  K irradiated by a FUV field and simultaneously by either CRs or X-rays. We suppose the radiation sources are extragalactic background or nearby other halos, rather than local ones in the same halo. In star-burst galaxies, although the internal radiation field can be very high, the interstellar media are expected to be metal-enriched. Since even a low level of metal enrichment ( $\gtrsim 10^{-5} Z_\odot$ ) induces fragmentation and prevents the SMS formation (Omukai, Schneider & Haiman 2008), we do not consider here the cases of internal sources.

The evolution during the gravitational collapse is calculated by a one-zone model (e.g., Omukai 2001). The actual hydrodynamical collapse of self-gravitating clouds is well described by the Penston-Larson self-similar solution (Penston 1969; Larson 1969). In this solution, the clouds consist of two spatial parts: the flat central core, whose size is about

the Jeans length  $\lambda_J$  and where number density of hydrogen nuclei  $n_H$ , temperature  $T$ , chemical concentrations of species  $i$ ,  $y(i)$ , etc. are nearly homogeneous, and the envelope, where the density profile obeys the power law with radius as  $\rho \propto r^{-2}$ . The central density increases approximately at the free-fall rate. In our one-zone model, all the physical variables such as  $n_H$ ,  $T$ , etc. are intended to indicate those at the center of the core. It has been confirmed that the thermal evolution of primordial clouds under strong FUV fields but without X-ray/CR ionization by the one-zone model reproduces very well that by the full three-dimensional calculation (Shang et al. 2010).

Our main interest in this paper is put on the cases with extremely strong FUV radiation, where  $H_2$  is totally dissociated and its cooling is quenched. To start gravitational collapse, such halos must be as massive as with its virial temperature  $\gtrsim 10^4$  K, where the H atomic cooling is effective. This requires the total mass of the halo being  $\gtrsim 2 \times 10^7 M_\odot$ , corresponding to  $\gtrsim 4 \times 10^6 M_\odot$  of gas for the virialization epoch  $z_{\text{vir}} \simeq 10$ . Since the pressure effect is not important in such massive halos, the baryonic density in the clouds  $\rho$  is assumed to increase with the free-fall timescale:

$$\frac{d\rho}{dt} = \frac{\rho}{t_{\text{ff}}}, \quad (1)$$

where  $t_{\text{ff}} = \sqrt{3\pi/32G\rho}$ . In evaluating  $t_{\text{ff}}$ , we neglect the contribution from the dark matter. The dark-matter gravity dominates that by the gas and shortens the collapse timescale only just after the virialization, where the temperature increases adiabatically in any case. We confirmed from experiments that the omission of dark-matter gravity does not cause any noticeable deviations in temperature evolution as a function of density.

The temperature evolution is calculated by solving the energy equation:

$$\frac{de}{dt} = -p \frac{d}{dt} \left( \frac{1}{\rho} \right) - \frac{\Lambda_{\text{net}}}{\rho}, \quad (2)$$

where  $e$  is the internal energy per unit mass,

$$e = \frac{1}{\gamma_{\text{ad}} - 1} \frac{k_B T}{\mu m_H}, \quad (3)$$

$p$  is the pressure,

$$p = \frac{\rho k_B T}{\mu m_H}, \quad (4)$$

$\mu$  is the mean molecular weight,  $k_B$  is the Boltzmann constant,  $\gamma_{\text{ad}}$  is the ratio of specific heat and  $\Lambda_{\text{net}}$  is the net cooling rate per unit volume. We set  $\mu = 1.2$  and  $\gamma_{\text{ad}} = 5/3$  in our calculation. The net cooling rate consists of the following contributions:

$$\Lambda_{\text{net}} = \Lambda_H + \Lambda_{H_2} + \Lambda_{HD} + \Lambda_{\text{chem}} - \Gamma_{\text{CR}} - \Gamma_X, \quad (5)$$

where  $\Lambda_H$ ,  $\Lambda_{H_2}$  and  $\Lambda_{HD}$  are the radiative cooling rates by H atom,  $H_2$  molecule and HD molecule, respectively,  $\Lambda_{\text{chem}}$  is the net cooling rate associated with chemical reactions, and  $\Gamma_{\text{CR}}$  and  $\Gamma_X$  are the heating rates by CRs and X-rays, respectively. In the metal-free gas, H cooling by Ly  $\alpha$  and two-photon emissions is effective at temperature  $\gtrsim 8000$  K, while  $H_2$  molecule is an important coolant at lower temperature. At even lower temperature  $\lesssim 150$  K, HD molecule becomes the dominant coolant. Such low temperature environment is realized for example in the case of ionization by intense

CRs or X-rays, which promotes  $H_2$  formation via electron catalysed reactions, and thereby lowering the temperature below  $\simeq 150$  K. The H atomic cooling rate is calculated by solving the level populations as in Omukai (2001), while, for the  $H_2$  and HD cooling rate, we adopt the fitting formulae by Galli & Palla (1998). In our calculation, we neglect the radiative cooling by He species, which is only effective for  $T \gtrsim 10^5$  K. The methods of calculation for heating rates by CRs and X-rays are described in Section 2.4.2 and 2.4.3, respectively.

When the density increases and the cloud becomes optically thick, the intensities of external radiation, i.e., FUV, CRs and X-rays, are attenuated before reaching the center and also the radiative cooling by e.g. H Ly  $\alpha$  and  $H_2$  becomes ineffective by the self-absorption. We assume the radius of the central core  $R_c$  is a half of the Jeans length  $\lambda_J$ ;

$$R_c = \frac{\lambda_J}{2} = \frac{1}{2} \sqrt{\frac{\pi k_B T}{G \rho \mu m_H}}. \quad (6)$$

Since we focus on the center of collapsing clouds, the column number density of  $i$ -th chemical species is

$$N(i) = y(i) n_H R_c. \quad (7)$$

We use this column density in considering the optical-depth effect on the incident radiation intensities, as well as on the radiative cooling rates.

## 2.2 chemistry

We consider the chemical reactions in primordial gas among the following 14 species: H,  $H_2$ ,  $e^-$ ,  $H^+$ ,  $H_2^+$ ,  $H^-$ , D, HD,  $D^+$ ,  $HD^+$ ,  $D^-$ , He,  $He^+$ , and  $He^{++}$ . The included reactions are summarized in Table 1. The following points are worth noting. We adopt the  $H_2$  collisional dissociation rate (reaction 7) of Martin, Schwarz & Mandy (1996), which is ten times larger than the older rate of Shapiro & Kang (1987) used by Omukai (2001) around  $\simeq 10^3 \text{ cm}^{-3}$ . Shang et al. (2010) found that this difference affects the value of the critical FUV flux  $J_{\text{crit}}$  by about an order of magnitude. For the photoionization of H (reactions 21 – 25) and the photodissociation of  $H_2^+$  (reaction 20), those from the excited levels are also included as in Omukai (2001).

## 2.3 Initial condition

The calculation starts at  $n_H = 0.1 \text{ cm}^{-3}$ , with initial temperature  $T = 160$  K, appropriate for halos virializing at  $z_{\text{vir}} = 10$ , whose turnaround epoch corresponds to  $z_{\text{turn}} \simeq 17$  (Omukai et al. 2008). The early stages at densities  $n_H = 0.1 \text{ cm}^{-3}$  and  $1.0 \text{ cm}^{-3}$  correspond to redshifts of  $z \simeq 15.5$  and 11.5, respectively. The initial concentrations of electron,  $y(e^-) = 2 \times 10^{-4}$ , and  $H_2$  molecule,  $y(H_2) = 2 \times 10^{-6}$ , are taken from the values at  $\sim 0.1 \text{ cm}^{-3}$  of Bromm & Loeb (2003). We set the initial He concentration at  $y(\text{He}) = 0.08$ , which corresponds to the He mass fraction,  $Y_{\text{He}} = 0.24$ .

## 2.4 Incident FUV radiation, CRs, and X-rays

### 2.4.1 FUV radiation

The incident FUV radiation field  $J_{\text{FUV}}(\nu)$  is assumed to have a diluted thermal spectrum, i.e.,  $J_{\text{FUV}}(\nu) \propto B_\nu(T_*)$ ,

**Table 1.** Chemical Reactions

Number	Reaction	Reference
H collisional reactions		
1	$\text{H} + \text{e}^- \rightarrow \text{H}^+ + 2\text{e}^-$	1
2	$\text{H}^+ + \text{e}^- \rightarrow \text{H} + \gamma$	3*
3	$\text{H} + \text{e}^- \rightarrow \text{H}^- + \gamma$	2
4	$\text{H}^- + \text{H} \rightarrow \text{H}_2 + \text{e}^-$	2
5	$\text{H} + \text{H}^+ \rightarrow \text{H}_2^+ + \gamma$	2
6	$\text{H}_2^+ + \text{H} \rightarrow \text{H}_2 + \text{H}^+$	2
7	$\text{H}_2 + \text{H} \rightarrow 3\text{H}$	4
8	$\text{H}_2 + \text{H}^+ \rightarrow \text{H}_2^+ + \text{H}$	2
9	$\text{H}_2 + \text{e}^- \rightarrow 2\text{H} + \text{e}^-$	2
10	$\text{H}^- + \text{e}^- \rightarrow \text{H} + 2\text{e}^-$	1
11	$\text{H}^- + \text{H}^+ \rightarrow 2\text{H}$	2
12	$\text{H}^- + \text{H}^+ \rightarrow \text{H}_2^+ + \text{e}^-$	2
13	$\text{H}_2^+ + \text{e}^- \rightarrow 2\text{H}$	2
14	$\text{H}_2^+ + \text{H}^- \rightarrow \text{H}_2 + \text{H}$	1
15	$3\text{H} \rightarrow \text{H}_2 + \text{H}$	5
16	$2\text{H} + \text{H}_2 \rightarrow 2\text{H}_2$	5
17	$2\text{H}_2 \rightarrow 2\text{H} + \text{H}_2$	5
photo-, and CR reactions		
18	$\text{H}_2 + \gamma \rightarrow 2\text{H}$	6
19	$\text{H}^- + \gamma \rightarrow \text{H} + \text{e}^-$	7
20	$\text{H}_2^+ + \gamma \rightarrow \text{H} + \text{H}^+$	8
21 – 25	$\text{H}(n) + \gamma \rightarrow \text{e}^- + \text{H}^+ \quad (n = 1 - 5)$	9
26	$\text{H} + \text{CR} \rightarrow \text{e}^- + \text{H}^+$	10
D reactions		
27	$\text{D}^+ + \text{e}^- \rightarrow \text{D} + \gamma$	11
28	$\text{D} + \text{H}^+ \rightarrow \text{D}^+ + \text{H}$	12
29	$\text{D}^+ + \text{H} \rightarrow \text{H}^+ + \text{D}$	12
30	$\text{D} + \text{H} \rightarrow \text{HD} + \gamma$	11
31	$\text{D} + \text{H}_2 \rightarrow \text{H} + \text{HD}$	11
32	$\text{HD}^+ + \text{H} \rightarrow \text{H}^+ + \text{HD}$	11
33	$\text{D}^+ + \text{H}_2 \rightarrow \text{H}^+ + \text{HD}$	13
34	$\text{HD} + \text{H} \rightarrow \text{H}_2 + \text{D}$	11
35	$\text{HD} + \text{H}^+ \rightarrow \text{H}_2 + \text{D}^+$	13
36	$\text{D} + \text{H}^+ \rightarrow \text{HD}^+ + \gamma$	11
37	$\text{D}^+ + \text{H} \rightarrow \text{HD}^+ + \gamma$	11
38	$\text{HD}^+ + \text{e}^- \rightarrow \text{H} + \text{D}$	11
39	$\text{D} + \text{e}^- \rightarrow \text{D}^- + \gamma$	11
40	$\text{D}^+ + \text{D}^- \rightarrow 2\text{D}$	11
41	$\text{H}^+ + \text{D}^- \rightarrow \text{D} + \text{H}$	11
42	$\text{H}^- + \text{D} \rightarrow \text{H} + \text{D}^-$	11
43	$\text{D}^- + \text{H} \rightarrow \text{D} + \text{H}^-$	11
44	$\text{D}^- + \text{H} \rightarrow \text{HD} + \text{e}^-$	11
45	$\text{HD} + \gamma \rightarrow \text{H} + \text{D}$	6
He reactions		
46	$\text{He} + \text{e}^- \rightarrow \text{He}^+ + 2\text{e}^-$	1
47	$\text{He}^+ + \text{e}^- \rightarrow \text{He} + \gamma$	1
48	$\text{He}^+ + \text{e}^- \rightarrow \text{He}^{++} + 2\text{e}^-$	1
49	$\text{He}^{++} + \text{e}^- \rightarrow \text{He}^+ + \text{H}^+ + \gamma$	1
50	$\text{He}^+ + \text{H} \rightarrow \text{He} + \text{H}^+ + \gamma$	14
51	$\text{He} + \text{H}^+ \rightarrow \text{He}^+ + \text{H}$	14
52	$\text{He} + \gamma \rightarrow \text{He}^+ + \text{e}^-$	1

(1) Abel et al. (1997); (2) Galli & Palla (1998); (3) Ferland et al. (1992; Case B); (4) Martin et al. (1996); (5) Palla, Salpeter & Stahler (1983); (6) Wolcott-Green & Haiman (2011); (7) John (1988); (8) Stancil (1994); (9) Rybicki & Lightman (1979); (10) Stacy & Bromm (2007); (11) Nakamura & Umemura (2002); (12) Savin (2002); (13) Galli & Palla (2002); (14) Yoshida et al. (2006).

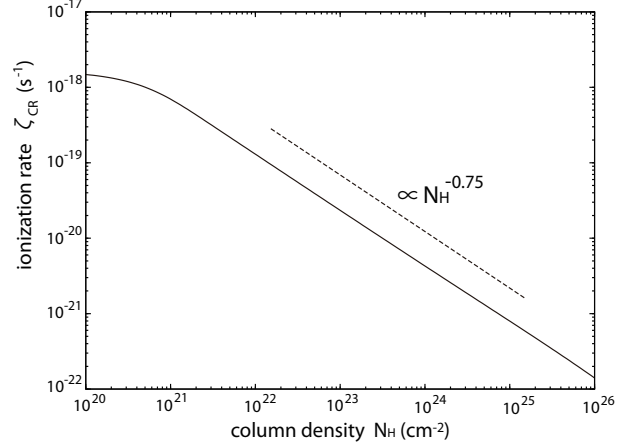


**Figure 1.** The cosmic-ray ionization rate  $\zeta_{\text{CR}}$  for  $U_{\text{CR}} = 10^{-15}$  erg cm $^{-3}$  and  $\epsilon_{\text{min}} = 10^6$  eV, and  $\epsilon_{\text{max}} = 10^{15}$  eV as a function of H column density  $N_{\text{H}}$ . In the high column-density limit, the rate is approximated as  $\zeta_{\text{CR}} \propto N_{\text{H}}^{-0.75}$ .

with brightness temperature  $T_* = 10^4$  or  $10^5$  K, corresponding to that from assembly of metal-enriched stars or massive Pop III stars, respectively. The normalization of the intensity is set at the Lyman-limit frequency  $\nu_{\text{L}} = 13.6$  eV by  $J_{21} = J_{\text{FUV}}(\nu)/10^{-21}$  erg s $^{-1}$  cm $^{-2}$  sr $^{-1}$  Hz $^{-1}$ . For the same value of  $J_{21}$  at the Lyman limit, the rate of H $_2$  photodissociation, which proceeds via absorption of photons of 11.2 – 13.6 eV does not vary so much for different values of  $T_*$ . On the other hand, H $^-$  photodissociation rate, whose threshold energy (0.755 eV) is far below the Lyman limit, is significantly affected with change of  $T_*$  even with the same  $J_{21}$ . For example, this rate is  $2 \times 10^4$  times higher for  $T_* = 10^4$  K than that for  $T_* = 10^5$  K with the same  $J_{21}$ . Since H $^-$  is the intermediary in the H $_2$ -forming reaction (reactions 3 and 4), the H $_2$  concentration depends sensitively on  $T_*$  (see Section 4).

The H $_2$  and HD are self-shielded against photodissociation for their column densities  $\gtrsim 10^{13}$  cm $^{-2}$ . The HD shielding is also contributed by H and H $_2$ . We use the shielding factors by Wolcott-Green & Haiman (2011).

#### 2.4.2 Cosmic Rays

For the incident CR flux, we follow the treatment by Stacy & Bromm (2007). The CR energy distribution  $dn_{\text{CR}}/d\epsilon$  (cm $^{-3}$  eV $^{-1}$ ) is assumed to obey a power-law spectrum with index  $-2$ , the value by the diffusive shock acceleration by a strong shock (e.g. Bell 1978) from the minimum energy  $\epsilon_{\text{min}} = 10^6$  eV to the maximum  $\epsilon_{\text{max}} = 10^{15}$  eV. After incident to the gas, CRs propagate inward with losing their energies by ionization up to the penetration depth  $D_{\text{p}}$  at a rate  $(d\epsilon/dt)_{\text{ion}}$ , for which we use the expression by Schlickeiser (2002). The heating rate by CRs at depth  $D$  is

$$\Gamma_{\text{CR}}(D) = \frac{E_{\text{heat}}}{\Delta\epsilon} \int_{\epsilon_{\text{min}}}^{\epsilon_{\text{max}}} \left( \frac{d\epsilon}{dt} \right)_{\text{ion}} \frac{dn_{\text{CR}}}{d\epsilon} e^{-D/D_{\text{p}}} d\epsilon, \quad (8)$$

where  $\Delta\epsilon = 50$  eV is the approximate kinetic energy of a CR particle lost upon each scattering (Spitzer & Tomasko

1968), and the ionization rate is

$$\zeta_{\text{CR}}(D) = \frac{\Gamma_{\text{CR}}(D)}{n_{\text{H}} E_{\text{heat}}}, \quad (9)$$

where  $E_{\text{heat}} \simeq 6$  eV is the energy deposited as heat per ionization in a neutral medium (Spitzer & Scott 1969; Shull & van Steenberg 1985). Note that the CR ionization rate is related with the total CR energy density,

$$U_{\text{CR}} = \int_{\epsilon_{\text{min}}}^{\epsilon_{\text{max}}} \epsilon \frac{dn_{\text{CR}}}{d\epsilon} d\epsilon, \quad (10)$$

by

$$\zeta_{\text{CR}} = 1.7 \times 10^{-18} U_{15} \text{ s}^{-1}, \quad (11)$$

in the low column density limit, where  $U_{15} = U_{\text{CR}}/10^{-15}$  erg cm<sup>-3</sup>. In Fig. 1, we also plot the CR ionization rate  $\zeta_{\text{CR}}$  as a function of the column density  $N_{\text{H}}$ . This can be approximated as

$$\begin{aligned} \zeta_{\text{CR}} &= 1.3 \times 10^{-19} U_{15} \left( \frac{N_{\text{H}}}{10^{22} \text{ cm}^{-2}} \right)^{-3/4} \text{ s}^{-1}, \\ &= 6.8 \times 10^{-20} U_{15} \left( \frac{n_{\text{H}}}{10^3 \text{ cm}^{-3}} \cdot \frac{T}{8000 \text{ K}} \right)^{-3/8} \text{ s}^{-1}, \end{aligned} \quad (12)$$

for column density higher than  $\gtrsim 10^{22}$  cm<sup>-2</sup>.

The CR ionization rate in the Milky Way has been estimated by many authors, including  $\zeta_{\text{CR}} \simeq 4 \times 10^{-16}$  s<sup>-1</sup> (Hayakawa, Nishimura & Takayanagi 1961),  $6.8 \times 10^{-18}$  s<sup>-1</sup>  $\lesssim \zeta_{\text{CR}} \lesssim 1.2 \times 10^{-15}$  s<sup>-1</sup> (Spitzer & Tomasko 1968) and  $\zeta_{\text{CR}} \simeq 3 \times 10^{-17}$  s<sup>-1</sup> (Webber 1998). By recent observation of H<sub>3</sub><sup>+</sup> in the interstellar medium, the average H<sub>2</sub> ionization by CRs is evaluated  $\zeta_{\text{CR},\text{H}_2} \simeq 4 \times 10^{-16}$  s<sup>-1</sup> (McCall et al. 2003; Indriolo et al. 2007), which is translated to a rather high H ionization rate of  $\zeta_{\text{CR}} \simeq 2.6 \times 10^{-16}$  s<sup>-1</sup>. The CR intensity at high redshift is totally uncertain. The CR energy density is set by a balance between the injection and the diffusive leakage. On one hand, star formation in young galaxies can be more active than in the Milky Way. The CR injection rate being proportional to the star formation rate, the gas in the neighborhood of such galaxies is subject to intense CRs. On the other hand, magnetic fields are expected to be much weaker in young galaxies, which results in the longer Larmor radii of CRs and easier leakage from the galaxies. This may result in weaker CR density if the CR sources are in the same halo. Considering those uncertainties, we here regard the CR energy density as a free parameter and calculate the cases for  $10^{-3} \leq U_{15} \leq 10^4$ , which corresponds to the CR ionization rate of  $10^{-21}$  s<sup>-1</sup>  $\lesssim \zeta_{\text{CR}} \lesssim 10^{-14}$  s<sup>-1</sup> in the low density case.

### 2.4.3 X-rays

Since the ionization cross sections of hydrogen and helium fall as  $\sigma_{\text{H}}(\nu) \propto \nu^{-3}$  and  $\sigma_{\text{He}}(\nu) \propto \nu^{-2}$ , respectively, towards higher energy photons, the soft X-ray (2 – 10 keV) photons reach far longer distance from the sources than ionizing UV photons. Many sources contribute to X-rays at a given point, i.e., an extragalactic X-ray background is built up (Haiman, Rees & Loeb 1997).

Following Glover & Brand (2003), we assume the incident X-ray background having a power-law spectrum with

index  $-1.5$ ,

$$J_{\text{X}}(\nu) = J_{\text{X},21} \times 10^{-21} \left( \frac{\nu}{\nu_0} \right)^{-1.5} \text{ erg s}^{-1} \text{ cm}^{-2} \text{ sr}^{-1} \text{ Hz}^{-1}, \quad (13)$$

where  $h\nu_0 = 1$  keV. We consider the X-ray ionization of both H and He atoms. The heating rate by X-rays is

$$\Gamma_{\text{X}} = \Gamma_{\text{X,H}} + \Gamma_{\text{X,He}}, \quad (14)$$

where

$$\Gamma_{\text{X},i} = \int \frac{4\pi J_{\text{X}}(\nu)}{h\nu} e^{-\tau\nu} \sigma_i(\nu) E_{\text{h},i} d\nu \quad (i = \text{H, He}), \quad (15)$$

the optical depth is given by

$$\tau\nu = N_{\text{H}}\sigma_{\text{H}}(\nu) + N_{\text{He}}\sigma_{\text{He}}(\nu), \quad (16)$$

$E_{\text{h},i}$  is the energy deposited as heat for each ionization process, and given by a formula by Wolfire et al. (1995). The ionization rate is also expressed as

$$\zeta_{\text{X},\text{p}}^i = \int \frac{4\pi J_{\text{X}}(\nu)}{h\nu} e^{-\tau\nu} \sigma_i(\nu) d\nu, \quad (17)$$

where the subscript p represents primary ionization by X-rays. The primary electron's energy is deposited not only in heating but also in the secondary ionization. Since the energy of the primary electron is far larger than the ionization threshold, the secondary ionization is more effective than the primary in the case of X-ray ionization. The secondary ionization rate of H is given by

$$\zeta_{\text{X},\text{s}}^{\text{H}} = \left( \zeta_{\text{X},\text{p}}^{\text{H}} + \frac{y(\text{He})}{y(\text{H})} \zeta_{\text{X},\text{p}}^{\text{He}} \right) \langle \phi^{\text{H}} \rangle, \quad (18)$$

and the secondary ionization rate of He is expressed similarly, where  $\langle \phi^{\text{H}} \rangle$  is the number of secondary ionization per primary electron averaged over the X-ray spectrum, for which we use the expression by Wolfire et al. (1995). Then, the terms on the right hand side mean the secondary ionization rate by primary electrons due to H and He ionization, respectively. The total ionization rate by X-rays is given by the sum of the primary and secondary rates:

$$\zeta_{\text{X}}^i = \zeta_{\text{X},\text{p}}^i + \zeta_{\text{X},\text{s}}^i \quad (i = \text{H, He}). \quad (19)$$

In considering the secondary ionization, the H and He ionization rates are about the same magnitudes,  $\zeta_{\text{X}}^{\text{H}} \simeq \zeta_{\text{X}}^{\text{He}}$ . We add the ionization rate by X-rays  $\zeta_{\text{X}}^{\text{H}}$  ( $\zeta_{\text{X}}^{\text{He}}$ ) to the photoionization rate  $k_{21}$  ( $k_{52}$ , respectively).

## 3 RESULTS

We here present the results of our calculation and describe the physical processes determining the thermal evolution of the clouds.

### 3.1 Effects of cosmic rays

In Fig. 2, we show the temperature evolution of collapsing clouds irradiated by FUV fields with a diluted blackbody spectrum  $T_* = 10^4$  K, along with CRs with energy density (a)  $U_{15} = 10^{-3}$ , (b) 1, (c) 10, and (d) 100. The lines in each panel are for cases with different values of FUV strength  $J_{21}$ , which are indicated by numbers in the panel. For the cases with  $U_{15} = 10^{-3}$ , 1, and 100, we also plot in Figs 3, 4, and

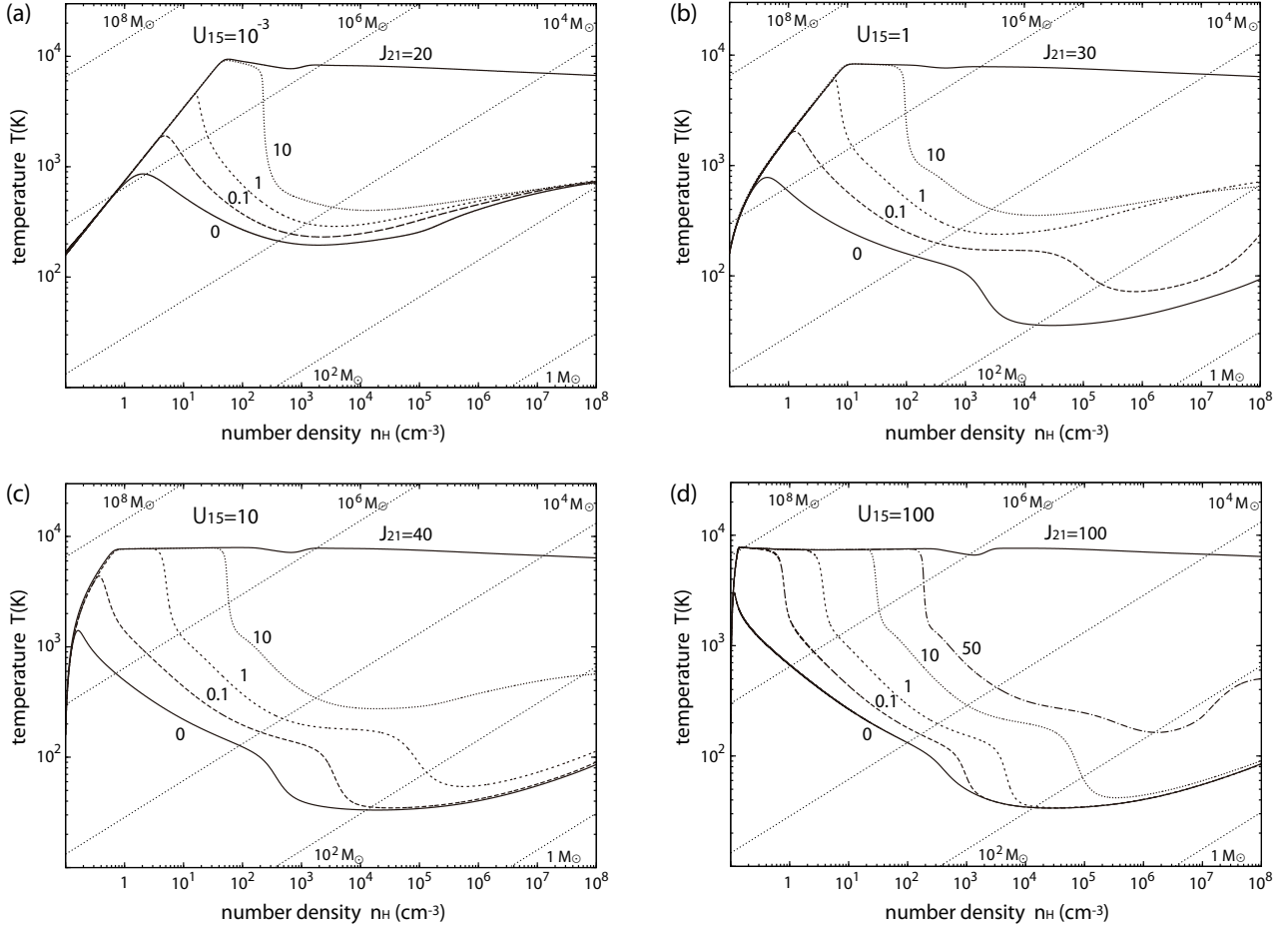


**Figure 2.** Effect of cosmic rays on the temperature evolution of primordial-gas clouds under FUV irradiation with  $T_* = 10^4$  K. Four panels correspond to the evolutionary tracks with four different cosmic-ray energy densities:  $U_{15} = 10^{-3}$ , 1, 10 and 100, where  $U_{15} = U_{\text{CR}}/10^{-15}$  erg  $\text{cm}^{-3}$ . The curves in each panel are those for different FUV fluxes, whose intensities  $J_{21}$  are indicated by numbers. The diagonal dotted lines show those at the constant Jeans mass, whose values are indicated by numbers in the Figure.

5, respectively, the cooling and heating rates per unit mass by individual processes, i.e., heating rates by compression (thick), by CR (dashed) and by chemical reactions (short dash-dotted), and cooling rates by the  $\text{H}_2$  (thick dotted), by HD (dash dotted) and by H atom (dotted). Since the major cooling and heating processes for  $U_{15} = 10$  are very similar to those for  $U_{15} = 1$ , we do not repeat presenting them.

First we see the case of  $U_{15} = 10^{-3}$ , where the CR is too weak to affect any aspect in the evolution (Figs 2 a and 3). In the no-FUV case ( $J_{21} = 0$ ), the cloud collapses along the standard  $\text{H}_2$ -cooling track (e.g., Palla et al. 1983). Following the initial adiabatic rise up to  $\sim 1000$  K, the temperature starts decreasing owing to the  $\text{H}_2$  cooling, which is produced through the  $\text{H}^-$  channel (reactions 3 and 4), until the critical density  $\simeq 10^4 \text{ cm}^{-3}$ , where the  $\text{H}_2$  level-populations reach the local thermodynamic equilibrium (LTE) and the cooling rate per unit mass saturates. The temperature thereafter increases again gradually by the compressional heating towards higher density (Fig. 3 a). Addition of a FUV field affects the evolution in the following way. As seen in the cases with  $J_{21} = 0.1$  and 1, with increasing radiation intensity, the initial adiabatic phase continues until higher den-

sity and temperature, where the  $\text{H}_2$  column density becomes high enough for efficient self-shielding against photodissociation. Once the  $\text{H}_2$  cooling becomes effective, the temperature decreases and gradually converges to the track in the no-FUV case. For  $J_{21} = 10$ , before the onset of  $\text{H}_2$  cooling, the temperature reaches  $\simeq 8000$  K and stays almost constant around  $10^2 \text{ cm}^{-3}$  owing to the H Ly  $\alpha$  cooling (dotted line in Fig. 2 a). This short isothermal phase is followed by a rapid temperature drop by the  $\text{H}_2$  cooling (see also Fig. 3 b). As in the cases with lower FUV fields, the temperature converges towards the no-FUV track. When a FUV field exceeds a critical value  $J_{21} \geq J_{\text{crit}} \simeq 20$ , the temperature evolution is qualitatively altered (top solid line in Fig. 2 a; see also Fig. 3 c). The isothermal evolution at  $\simeq 8000$  K continues until very high density ( $\sim 10^{16} \text{ cm}^{-3}$ ) and the  $\text{H}_2$  cooling never becomes important. This bifurcation of thermal evolution originates from the fact that if the  $\text{H}_2$  formation is prevented until the critical density for LTE, sufficient  $\text{H}_2$  never forms because, at higher density, (i) the amount of  $\text{H}_2$  needed for cooling increases (ii) collisional dissociation from the excited ro-vibrational levels of  $\text{H}_2$  becomes effective, which reduces the  $\text{H}_2$  fraction (Omukai 2001).

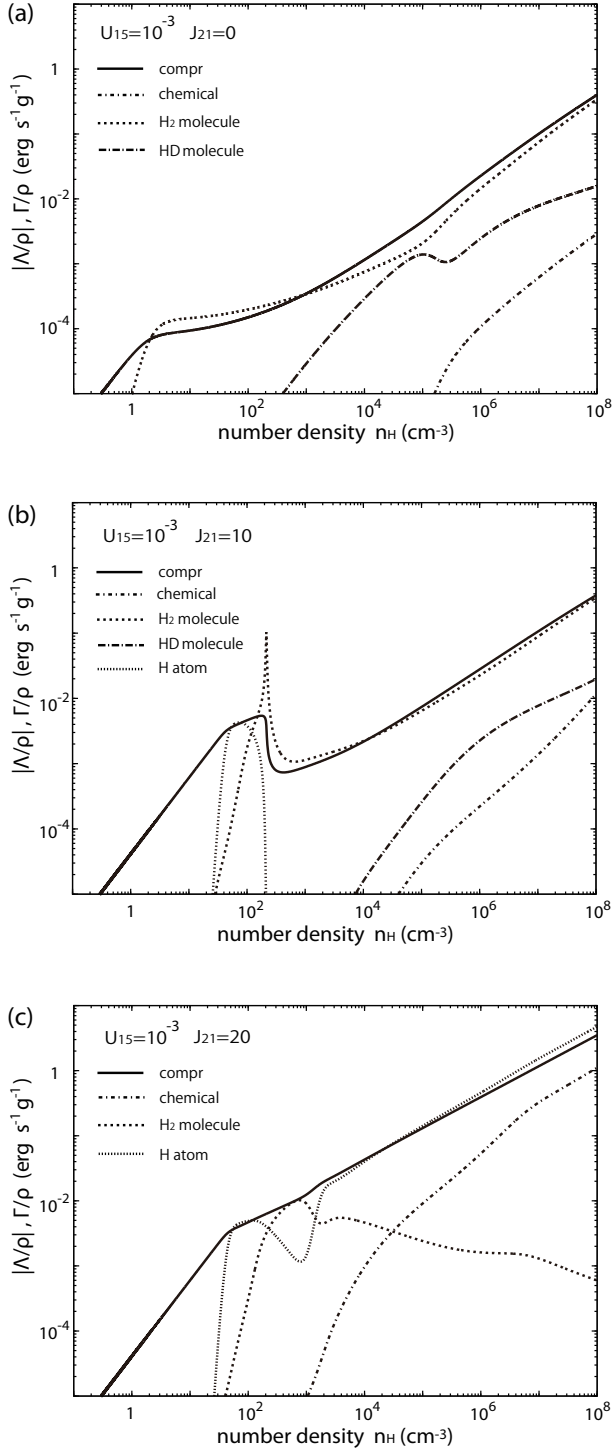


**Figure 3.** Cooling and heating rates per unit mass as a function of the central number density. The cosmic ray energy density is  $U_{15} = 10^{-3}$ , and the FUV intensity is (a)  $J_{21} = 0$ , (b)  $J_{21} = 10$  and (c)  $J_{21} = 20$  for  $T_* = 10^4$  K. The lines show the heating rates by compression (thick) and chemical reactions (short dash-dotted), and cooling rates by  $H_2$  (thick dotted) and HD (dash-dotted) molecules, H atoms (dotted).

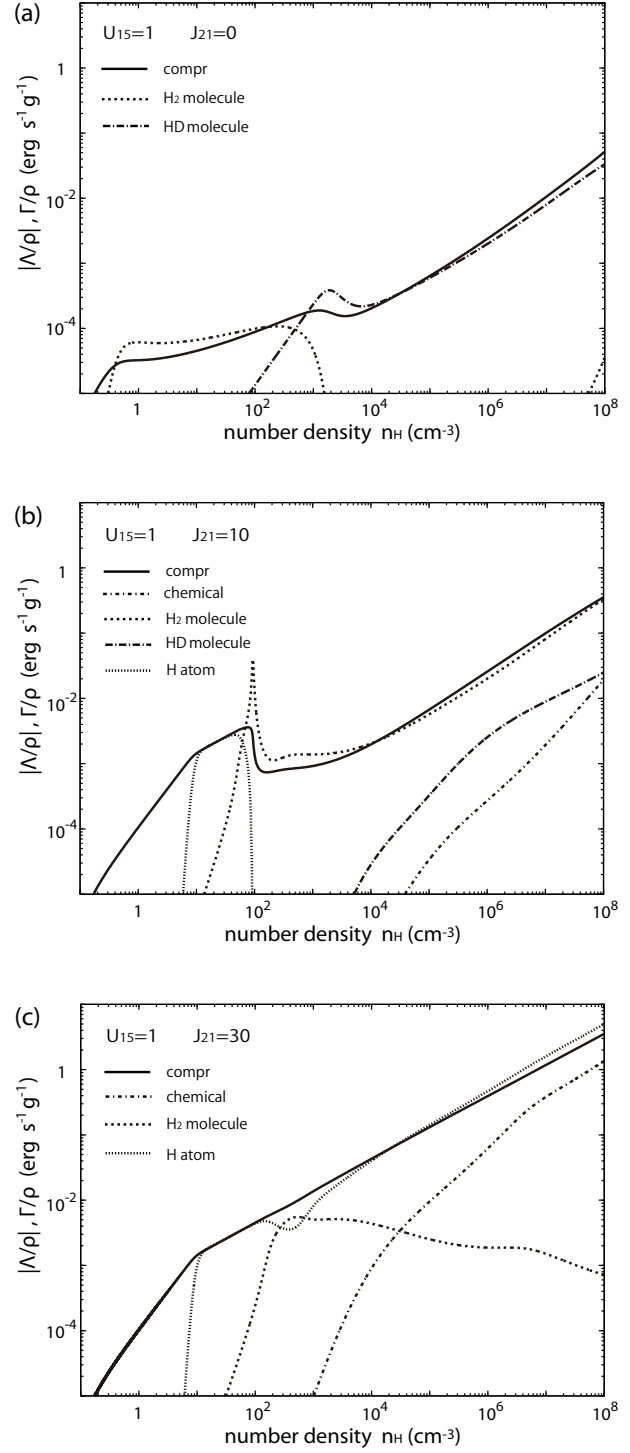


**Figure 4.** The same as Fig. 3, but for the cosmic ray energy density  $U_{15} = 1$ , and the FUV intensity (a)  $J_{21} = 0$ , (b)  $J_{21} = 10$  and (c)  $J_{21} = 30$ .

Next, we see how the thermal evolution described above changes with increasing CR flux. The CR effects are twofold, i.e., heating and ionization. The stronger the CR flux is, the more rapid is the initial temperature-increase owing to the CR heating as seen in Fig. 2 (b)–(d). In Fig. 5 for  $U_{15} = 100$ , very high CR-heating rate can be seen at the lowest density. Enhanced ionization degree facilitates the  $H_2$  formation via

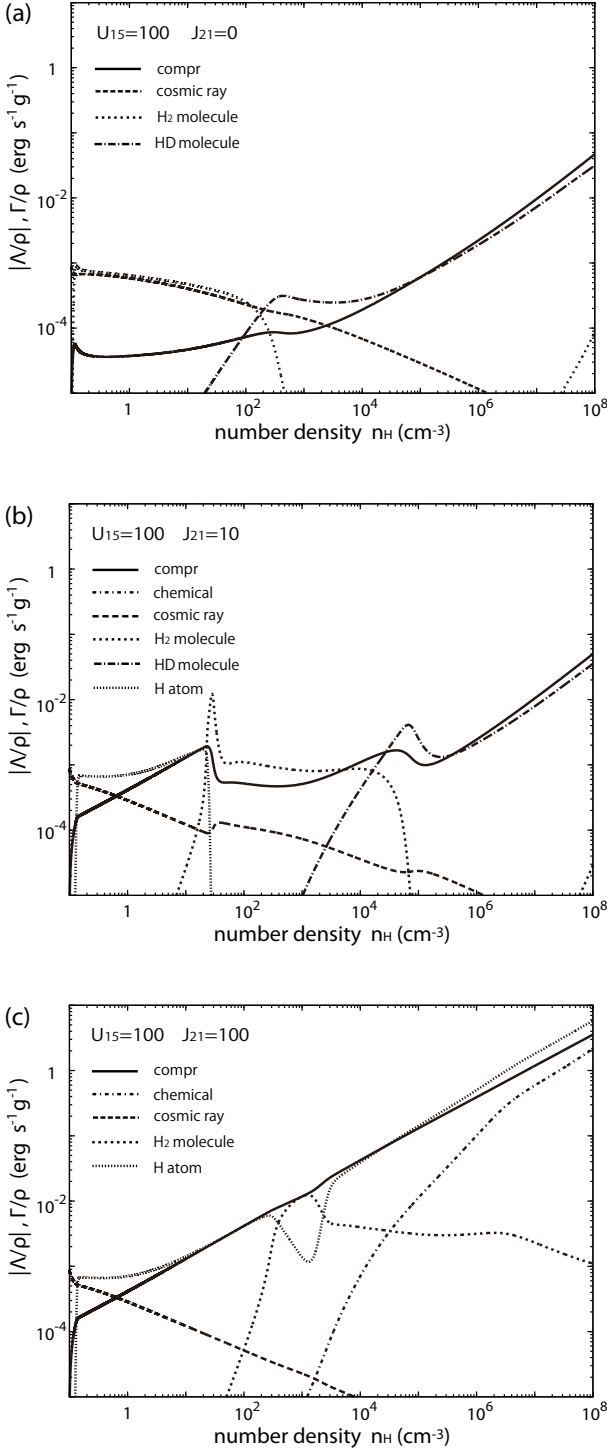


**Figure 5.** The same as Fig. 3, but for the cosmic ray energy density  $U_{15} = 100$ , and the FUV intensity (a)  $J_{21} = 0$ , (b)  $J_{21} = 10$  and (c)  $J_{21} = 100$ . In addition to cooling and heating rates shown in Fig. 4, heating rate by cosmic rays is also shown (dashed).

$H^-$  channel. To quench  $H_2$  cooling totally, higher FUV flux is necessary, namely, the value of the critical FUV flux  $J_{\text{crit}}$  becomes larger. For example, as seen in Fig. 2 (d), under a very strong CR field of  $U_{15} = 100$ , even such strong FUV flux as  $J_{21} = 50$  is not enough to quench the  $H_2$  cooling. In Fig. 6 (a), we plot the critical FUV flux  $J_{\text{crit}}$  as a function

of the CR intensity. In the case of  $T_* = 10^4$  K, from its low-CR limit of  $J_{\text{crit}} \simeq 20$ ,  $J_{\text{crit}}$  begins to increase around  $U_{15} \sim 10$  and continues increasing as  $J_{\text{crit}} \propto U_{15}^{1/2}$  in the high  $U_{15}$  limit. The dominant cooling and heating processes are similar in all cases of the FUV flux exceeding the critical value  $J_{\text{crit}}$  (see Figs 3 c, 4 c and 5 c).

For low FUV flux  $J_{21} \lesssim 0.1 - 10$ , the higher  $H_2$  concentration by CR ionization results in the lower temperature than in the no-CR case (see Fig. 2 b–d). This low temperature environment ( $\lesssim 150$  K) favors HD formation, and its cooling causes further temperature decrease to a few 10 K (e.g., Fig. 2 b–d for  $J_{21} = 0$ ). As seen in Fig. 4 (a), HD becomes the main cooling agent at high density and low temperature ( $n_H \gtrsim 10^3 \text{ cm}^{-3}$  and  $T \lesssim 150$  K). Without extra ionization, enough HD for cooling is not produced under FUV radiation with  $J_{21} \gtrsim 10^{-2}$  for  $T_* = 10^4$  K (Yoshida, Omukai & Hernquist 2007; Wolcott-Green & Haiman 2011). As seen in Figs 2 (b) and 4 (b), (c), for the case of  $U_{15} = 1$ , the FUV flux higher than  $J_{21} \gtrsim 1$  suppresses the HD cooling and the thermal evolution becomes the same as that for  $U_{15} = 10^{-3}$ . However, the presence of stronger CRs permits HD cooling despite of such a high FUV flux as  $J_{21} \gtrsim 10$  (see Fig. 5 b).

So far, we limit our analysis to the radiation spectra of  $T_* = 10^4$  K. We also studied the case of  $T_* = 10^5$  K. As mentioned in Section 2.4.1, the  $H^-$  photodissociation rate depends sensitively on the brightness temperature  $T_*$ . Then, the concentration of  $H_2$  produced through the  $H^-$  channel (reactions 3 and 4) changes with the value of  $T_*$ . This leads to the enhancement of the critical FUV flux  $J_{\text{crit}}$  for  $T_* = 10^5$  K compared to the case for  $T_* = 10^4$  K (see Section 4). The critical flux  $J_{\text{crit}}$  for  $T_* = 10^5$  K is also plotted in Fig. 6 (a). We find that  $J_{\text{crit}} = 1.6 \times 10^4$  for  $T_* = 10^5$  K, while  $J_{\text{crit}} = 20$  for  $T_* = 10^4$  K in the no-CR cases. For CR energy density higher than  $U_{15} \sim 10$ , the critical FUV flux  $J_{\text{crit}}$  increases as  $\propto U_{15}^{1/2}$  in both  $T_* = 10^4$  and  $10^5$  K cases.

### 3.2 Effects of X-rays

Here, we briefly mention the cases of the clouds irradiated both by FUV and X-rays. The temperature evolution is shown in Fig. 7 for (a)  $J_{X,21} = 10^{-6}$  and (b)  $10^{-2}$ . For the X-ray intensity as low as  $J_{X,21} = 10^{-6}$ , the effects of X-rays, either ionization or heating, are not important and the evolutionary tracks in Fig. 7 (a) are the same as those with negligible CRs ( $U_{15} = 10^{-3}$ ) in Fig. 2 (a). When the X-ray intensity is elevated to  $J_{X,21} = 10^{-2}$ , the gas is heated instantaneously (see Fig. 7 b). In the case of  $J_{21} = 0$ , the  $H_2$  cooling balances the X-ray heating at  $\simeq 5000$  K and the temperature begins decreasing thereafter. For  $J_{21} \geq 0.1$ , the temperature reaches at  $\simeq 8000$  K and remains almost constant for a while by the H atomic cooling until  $H_2$  is self-shielded against the FUV field. Similar to the case of CR ionization, X-ray ionization enhances the critical FUV flux  $J_{\text{crit}}$  for quenching the  $H_2$  cooling. This critical FUV flux  $J_{\text{crit}}$  is plotted in Fig. 6 (b) as a function of the X-ray intensity  $J_{X,21}$ . As in the case of CR ionization,  $J_{\text{crit}}$  remains constant below a threshold around  $J_{X,21} \sim 10^{-3}$  and increases as  $(J_{X,21})^{1/2}$  for higher X-ray intensity. Since the behaviors of temperature evolution for different FUV fluxes as well as the dominant cooling/heating processes are



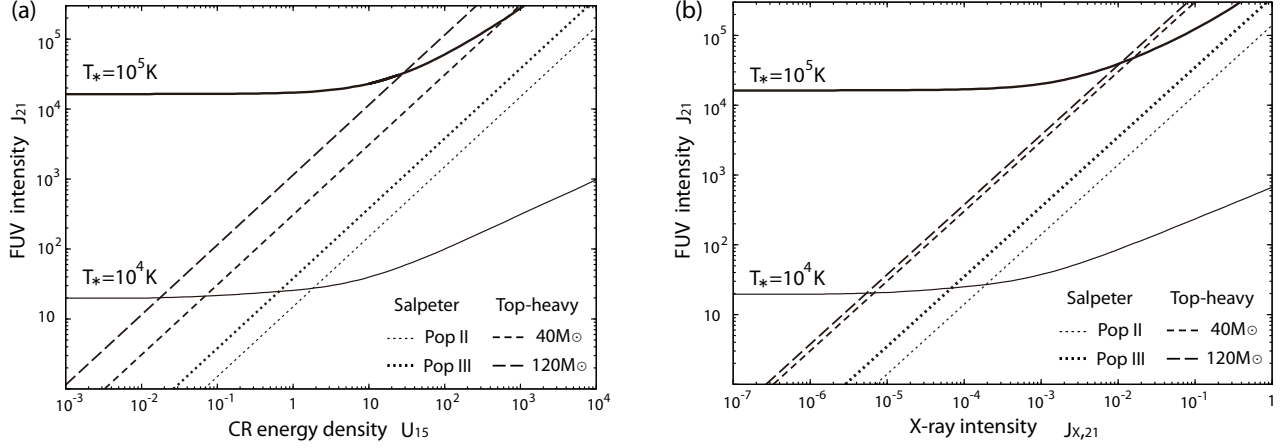


**Figure 6.** (a) The dependence of the critical FUV flux  $J_{\text{crit}}$  on the CR energy density  $U_{15}$  (solid curves) for two spectral types (thin curve:  $T_* = 10^4$  K, thick curve:  $T_* = 10^5$  K). In both cases,  $J_{\text{crit}} \propto U_{15}^{1/2}$  for  $U_{15} \gtrsim 10$ . The lines indicate the relations between  $J_{21}$  and  $U_{15}$  emitted from a star-forming galaxy (equation 36) with (i) the Salpeter IMF and  $Z = 10^{-3} Z_\odot$  (Pop II; thin dotted), (ii) Salpeter IMF and  $Z = 0$  (Pop III; thick dotted), (iii) the top-heavy IMF with  $m_{\text{OB}} = 40 M_\odot$  (short dashed) and (iv) the top-heavy IMF with  $120 M_\odot$  (long dashed), respectively. The intersection of the curves and lines for each  $T_*$  case corresponds to the actual CR energy density and critical FUV flux  $J_{\text{crit}}$  in a halo affected by the star-forming galaxy. (b) the same plot for the X-ray ionization. For both values of  $T_*$ ,  $J_{\text{crit}} \propto (J_{X,21})^{1/2}$  for  $J_{X,21} \gtrsim 10^{-3}$ . Note that the fraction of halos with  $\gtrsim 10^8 M_\odot$  at  $z = 10$  irradiated by FUV radiation  $J_{21}$  exceeding  $\gtrsim 10^5$  is negligibly low  $\lesssim 10^{-28}$ .

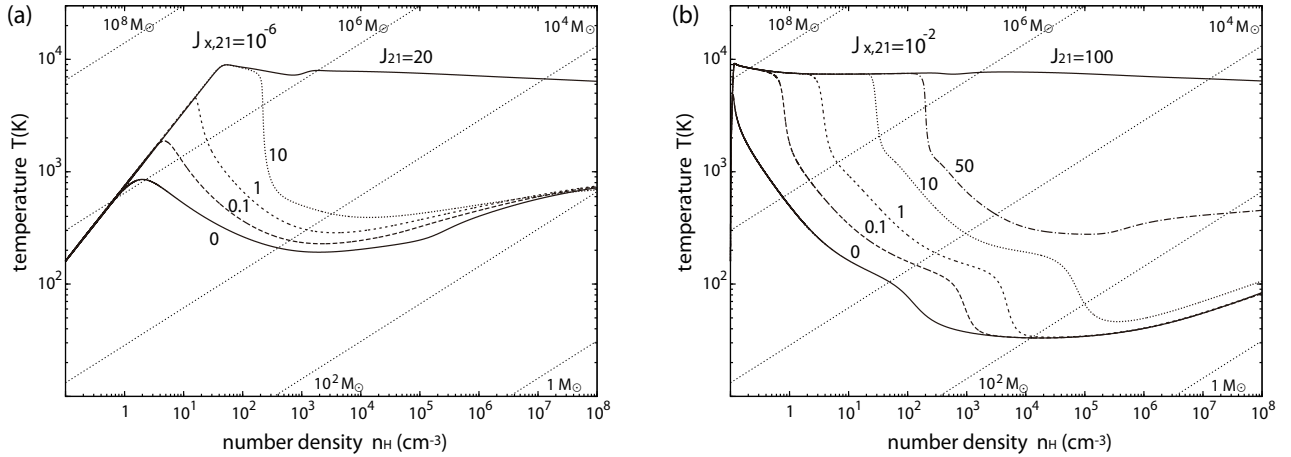


**Figure 7.** Effect of X-ray ionization on the temperature evolution of metal-free clouds under FUV irradiation with  $T_* = 10^4$  K. Two panels show the evolutionary tracks with two different X-ray intensities  $J_{X,21} = 10^{-6}$  and  $10^{-2}$ . The curves in each panel are those for different FUV fluxes, whose intensities  $J_{21}$  are indicated by numbers. The diagonal dotted lines show those at the constant Jeans mass, whose values are indicated by numbers in the Figure.

very similar to the cases with CRs, we do not repeat their description here.

#### 4 DEPENDENCE OF THE CRITICAL FUV FLUX ON CR/X-RAY INTENSITY

In Section 3, we see that strong CR and X-ray fluxes lead to the enhancement of the critical FUV flux as  $J_{\text{crit}} \propto U_{15}^{1/2}$  and  $\propto (J_{X,21})^{1/2}$ , respectively (see Fig. 6). Also,  $J_{\text{crit}}$  decreases with lowering FUV temperature  $T_*$ . In this section, we discuss the reason for these dependences.

In the cloud under a high enough FUV field, the tem-

perature reaches  $\simeq 8000$  K and remains constant by the H Ly $\alpha$  cooling. If sufficient H<sub>2</sub> to cool forms during this isothermal collapse, the temperature drops by its cooling and the isothermal evolution is terminated. Otherwise, the isothermal evolution continues until very high density of  $\sim 10^{16} \text{ cm}^{-3}$ , where the cloud becomes optically thick to the H<sup>-</sup> bound-free absorption (Omukai 2001). The H<sub>2</sub> concentration needed for its cooling to overcome the compressional heating is

$$y_{\text{cool}}(\text{H}_2) = \frac{(3/2)k_{\text{B}}T}{\mathcal{L}_{\text{H}_2}t_{\text{ff}}}, \quad (20)$$

where  $\mathcal{L}_{\text{H}_2} \equiv \Lambda_{\text{H}_2}/n(\text{H}_2)$  (erg s<sup>-1</sup>) is the cooling rate per an H<sub>2</sub> molecule. Since most hydrogen is in the atomic form during the isothermal collapse, we assume  $n(\text{H}) = n_{\text{H}}$  in this Section. In Fig. 8, we show  $y_{\text{cool}}(\text{H}_2)$  (thick solid line) as a function of density for the isothermal collapse at 8000 K. Since  $\mathcal{L}_{\text{H}_2}$  increases linearly with number density until the critical density for LTE  $n_{\text{H,cr}} \simeq 3 \times 10^3 \text{ cm}^{-3}$  (at 8000 K) and saturates for higher density,  $y_{\text{cool}}(\text{H}_2)$  decreases as  $\propto n_{\text{H}}^{-1/2}$  until  $n_{\text{H,cr}}$ , reaches the minimum  $\simeq 1.4 \times 10^{-7}$  there, and increases as  $\propto n_{\text{H}}^{1/2}$  for higher density. This  $y_{\text{cool}}(\text{H}_2)$  is to be compared with the actual amount of H<sub>2</sub> present  $y(\text{H}_2)$ . Before the temperature reaches  $\simeq 8000$  K, the H<sub>2</sub> concentration attains the equilibrium value set by the balance between the formation and destruction reactions. The effective rate coefficient of H<sub>2</sub> formation via H<sup>-</sup> channel taking account of the H<sup>-</sup> photodissociation is

$$k_{\text{form}} = k_3 \frac{k_4 n_{\text{H}}}{k_4 n_{\text{H}} + k_{19}}, \quad (21)$$

where

$$k_{19} = \beta_{19} J_{21}, \quad (22)$$

by using  $\beta_{19} = 2 \times 10^{-7}$  ( $1 \times 10^{-11}$ ) for  $T_* = 10^4$  K ( $10^5$  K, respectively). This H<sub>2</sub> is destroyed either by photodissociation (reaction 18), which is dominant at the low density where the FUV radiation is not shielded, or collisionally (reaction 7) at higher density. Equating the larger of those dissociation rates with the formation rate, we obtain the H<sub>2</sub> concentration

$$y(\text{H}_2) = \min(n_{\text{H}} k_{18}^{-1}, k_7^{-1}) k_{\text{form}} y(e^-) \\ \equiv \min(y_{\text{pd}}(\text{H}_2), y_{\text{cd}}(\text{H}_2)). \quad (23)$$

The photodissociation rate coefficient is written as

$$k_{18} = \beta_{18} J_{21}, \quad (24)$$

where  $\beta_{18} = 4.2 \times 10^{-12}$  ( $1.3 \times 10^{-12}$ ) for  $T_* = 10^4$  K ( $10^5$  K, respectively). In the above, we assume the cloud is transparent to the photodissociating radiation since  $y_{\text{pd}}(\text{H}_2)$  immediately exceeds  $y_{\text{cd}}(\text{H}_2)$  once the self-shielding becomes important. The values of  $y(\text{H}_2)$  by equation (23) are plotted in Fig. 8 for some combinations of  $T_*$  and  $J_{21}$  for the ionization degree  $y(e^-) = 4 \times 10^{-5}$ , corresponding the no-CR/X-ray case (see later). The almost vertical portion of  $y(\text{H}_2)$  on the low-density side is limited by the photodissociation ( $y_{\text{pd}}(\text{H}_2)$ ), while the gradually changing part at higher density is set by the collisional dissociation ( $y_{\text{cd}}(\text{H}_2)$ ). In the cases with  $J_{21} = 0.1$  and 1 ( $10^3$  and  $10^4$ ) for  $T_* = 10^4$  K ( $10^5$  K, respectively),  $y(\text{H}_2)$  exceeds  $y_{\text{cool}}(\text{H}_2)$  at some density. At this moment, the actual temperature falls from  $\simeq 8000$  K and the isothermal collapse terminates. On the other hand, in the case with  $J_{21} = 20$  ( $2 \times 10^4$ ) for  $T_* = 10^4$  K ( $10^5$  K, respectively),  $y(\text{H}_2)$  always remains below  $y_{\text{cool}}(\text{H}_2)$  and thus the isothermal collapse continues.

For density higher than the critical density  $n_{\text{H,cr}} \sim 10^3 \text{ cm}^{-3}$ , the H<sub>2</sub> concentration decreases owing to effective collisional dissociation from excited ro-vibrational levels and has no chance to reach  $y_{\text{cool}}(\text{H}_2)$  anymore. To initiate efficient H<sub>2</sub> cooling, H<sub>2</sub> concentration must exceed  $y_{\text{cool}}(\text{H}_2)$  before  $n_{\text{H,cr}}$ . Thus, we can find the critical flux  $J_{\text{crit}}$  by the condition whether  $y(\text{H}_2)$  at  $n_{\text{H,cr}} \sim 10^3 \text{ cm}^{-3}$  is higher than  $y_{\text{cool}}(\text{H}_2)$ .

In the case of irradiation with hard FUV spectra (as

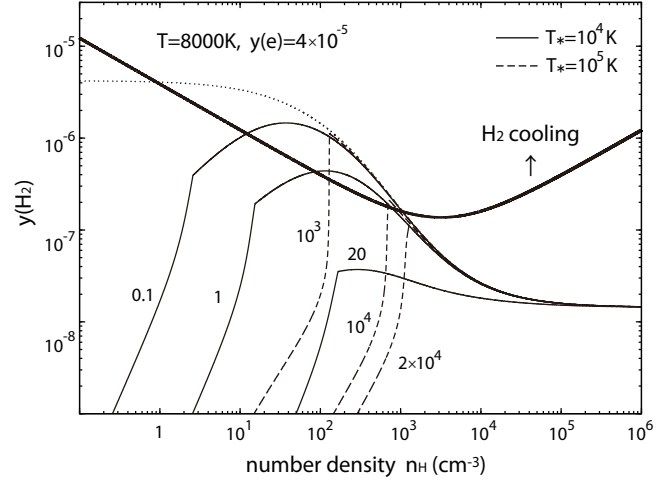


**Figure 8.** The H<sub>2</sub> concentration  $y(\text{H}_2)$  estimated by equation (23) (thin lines) vs. that needed for its cooling to exceed the compressional heating  $y_{\text{cool}}(\text{H}_2)$  (thick line) in the isothermally collapsing clouds at 8000 K with the ionization degree  $y(e^-) = 4 \times 10^{-5}$ . The H<sub>2</sub> concentrations are shown for the FUV fields with brightness temperatures  $T_* = 10^4$  K (thin solid lines) and  $10^5$  K (thin dashed lines). For each value of  $T_*$ , three cases with different FUV intensities  $J_{21}$ , which are indicated by numbers in the Figure, are presented. The dotted line shows  $y_{\text{cd}}(\text{H}_2)$  without H<sup>-</sup> photodissociation.

$T_* = 10^5$  K), photodissociation limits the H<sub>2</sub> concentration and H<sup>-</sup> photodissociation is relatively irrelevant (i.e.,  $k_{\text{form}} \simeq k_3$ ). From the condition  $y_{\text{pd}}(\text{H}_2) = y_{\text{cool}}(\text{H}_2)$  at  $n_{\text{H,cr}}$ , we obtain

$$J_{\text{crit}} = \frac{1}{\beta_{18}} \frac{k_3 n_{\text{H,cr}} y(e^-)}{y_{\text{cool}}(\text{H}_2)}. \quad (25)$$

On the other hand, for softer FUV spectra, (as  $T_* = 10^4$  K), the H<sub>2</sub> formation rate is significantly reduced by H<sup>-</sup> photodissociation:  $k_{\text{form}} = k_3 k_4 n_{\text{H}} / k_{19}$ . The dotted line in Fig. 8 shows  $y_{\text{cd}}(\text{H}_2)$  without H<sup>-</sup> photodissociation, which exceeds  $y_{\text{cool}}(\text{H}_2)$  before reaching  $n_{\text{H,cr}}$ . The actual value of  $y_{\text{cd}}(\text{H}_2)$  is, however, suppressed by H<sup>-</sup> photodissociation (see thin solid lines in Fig. 8) and thus the H<sub>2</sub> concentration is limited by collisional dissociation. Therefore, we obtain from the condition  $y_{\text{cd}}(\text{H}_2) = y_{\text{cool}}(\text{H}_2)$  at  $n_{\text{H,cr}}$ :

$$J_{\text{crit}} = \frac{k_4}{\beta_{19} k_7} \frac{k_3 n_{\text{H,cr}} y(e^-)}{y_{\text{cool}}(\text{H}_2)}. \quad (26)$$

In general, the critical FUV flux is given by the larger of the above two values (equations 25 and 26).

Note that  $J_{\text{crit}}$  increases with the ionization degree  $y(e^-)$ , which can be evaluated as follows. Without external ionization, the ionization degree is governed by

$$\frac{dy(e^-)}{dt} = -k_2 n_{\text{H}} y(e^-)^2. \quad (27)$$

Integrating this equation for a collapsing cloud (i.e., equation 1),

$$y(e^-) = \frac{y_0(e^-)}{1 + 2k_2 y_0(e^-) n_{\text{H}} t_{\text{ff}}}, \quad (28)$$

where  $y_0(e^-)$  is the initial ionization degree. For density  $\gtrsim 50 \text{ cm}^{-3}$ , this renders  $y(e^-) = (2k_2 n_{\text{H}} t_{\text{ff}})^{-1}$ . Equation (28)

gives  $y(e^-) \simeq 4 \times 10^{-5}$  at  $n_{\text{H}} = 10^3 \text{ cm}^{-3}$ . Using the values at  $10^3 \text{ cm}^{-3}$ , equations (25) and (26) lead to the critical FUV flux  $J_{\text{crit}} \sim 10 (10^4)$  for  $T_* = 10^4 \text{ K} (10^5 \text{ K}, \text{ respectively})$ , which are indeed similar to our numerical results for the no-CR/X-ray cases (Fig. 6).

In the presence of strong CRs, the ionization degree is set by the balance between recombination and CR ionization:

$$y(e^-) = \left( \frac{\zeta_{\text{CR}}}{k_2} \right)^{1/2} n_{\text{H}}^{-1/2}. \quad (29)$$

Comparing equations (28) and (29), we see that the CR ionization controls the ionization degree if its rate is higher than

$$\zeta_{\text{CR,crit}} = \frac{1}{4k_2 n_{\text{H}} t_{\text{ff}}^2} \simeq 3.8 \times 10^{-19} \text{ s}^{-1}, \quad (30)$$

where the last equation is evaluated at  $T = 8000 \text{ K}$ . This value is equivalent to the CR energy density  $U_{\text{CR,crit}} \simeq 5.5 \times 10^{-15} \text{ erg cm}^{-3}$  from equation (12). For  $U_{\text{CR}} \gtrsim U_{\text{CR,crit}}$ , the ionization degree, as well as the critical FUV flux, increases as  $\propto U_{\text{CR}}^{1/2}$ . This relation is reproduced well the behavior of  $J_{\text{crit}}$  as a function  $U_{15}$  shown in Fig. 6 (a).

Note that our critical CR density is similar to another threshold value where the HD cooling becomes important in the absence of FUV radiation,  $U_{\text{CR}} = 2 \times 10^{-15} \text{ erg cm}^{-3}$  (Stacy & Bromm 2007). This is not a coincidence: both critical values are related to enhancement of the ionization degree and thus  $\text{H}_2$  concentration from the case without CR ionization.

Next we consider the case of the X-ray ionization. Just the same as in the CR ionization, X-rays enhance the ionization degree as  $y(e^-) \propto (J_{\text{X},21})^{1/2}$  and thus  $J_{\text{crit}} \propto (J_{\text{X},21})^{1/2}$  for  $J_{\text{X},21} \gtrsim 10^{-3}$ , whose threshold is determined by the balance between recombination and X-ray ionization. This describes well the results shown in Fig. 6 (b).

Our value of  $J_{\text{crit}} = 20$  for  $T_* = 10^4 \text{ K}$  is smaller than  $J_{\text{crit}} = 39$  which Shang et al. (2010) estimated with one-zone model. This difference comes from the  $\text{H}_2$ -formation rate at high temperature: the rate coefficient we adopt (Galli & Palla 1998) is smaller than that Shang et al. (2010) used (Abel et al. 1997). On the other hand, our value of  $J_{\text{crit}} = 1.6 \times 10^4$  for  $T_* = 10^5 \text{ K}$  is slightly larger than Shang et al. (2010) because we use the new shielding factor by Wolcott-Green & Haiman (2011).

## 5 CR AND X-RAY FROM STAR-FORMING GALAXIES

So far, we have regarded the intensities of FUV, CRs and X-rays as free parameters in our calculation. All those radiation fields are, however, closely linked to the star-formation activity in galaxies and thus their intensities, i.e.,  $J_{21}$ ,  $U_{15}$  and  $J_{\text{X},21}$ , are all proportional to the star formation rate (SFR). We here consider the star-forming galaxies with two types of initial mass function (IMF): the Salpeter IMF and the top-heavy one. For the Salpeter IMF, we take the mass range of  $1 - 100 M_{\odot}$  and consider two cases of the stellar metallicity  $Z = 10^{-3} Z_{\odot}$  and 0, which corresponds to Pop II and III star clusters, respectively. For Pop III galaxies, we also consider the two cases of the top-heavy IMF where all

**Table 2.** The IMF models of star-forming galaxies

model	IMF	mass ( $M_{\odot}$ )	metallicity ( $Z_{\odot}$ )	$T_*$ (K)
(i)	Salpeter	1 – 100	$10^{-3}$	$10^4$
(ii)	Salpeter	1 – 100	0	$10^5$
(iii)	top-heavy	40	0	$10^5$
(iv)	top-heavy	120	0	$10^5$

stars are  $m_{\text{OB}} = 40 M_{\odot}$  or  $120 M_{\odot}$ . The IMF models we study are summarized in Table 2.

For FUV flux, we use the Lyman-Werner photon emissivity from a star-forming galaxy for the IMF models calculated by Schaerer (2002; 2003):

$$J_{21} = \left\{ \begin{array}{l} 6.5 \times 10^2 \\ 1.6 \times 10^3 \\ 1.4 \times 10^4 \\ 1.7 \times 10^4 \end{array} \right\} \left( \frac{d}{10 \text{ kpc}} \right)^{-2} \left( \frac{\text{SFR}}{20 M_{\odot} \text{ yr}^{-1}} \right), \quad (31)$$

where  $d$  is the distance from the source, and the numbers in the bracket correspond to the IMF models in the same order as in Table 2.

We assume that supernova remnants (SNRs) are the sources of CRs. The total CR energy from a SNR is written as (Stacy & Bromm 2007)

$$E_{\text{CR}} = 10^{51} \left( \frac{p_{\text{CR}}}{0.1} \right) \left( \frac{E_{\text{SN}}}{10^{52} \text{ erg}} \right) \text{ erg}, \quad (32)$$

where  $p_{\text{CR}}$  is the fraction of SN explosion energy  $E_{\text{SN}}$  going into the CR energy. Using the supernova rate in the source galaxy

$$\dot{N}_{\text{SN}} = \frac{f_{\text{OB}} \text{SFR}}{\bar{m}_{\text{OB}}}, \quad (33)$$

where  $f_{\text{OB}}$ ,  $\bar{m}_{\text{OB}}$  is the mass fraction and average mass of massive ( $\geq 8 M_{\odot}$ ) stars, the CR energy density of  $U_{\text{CR}}$  is

$$U_{\text{CR}} = \dot{N}_{\text{SN}} \frac{E_{\text{CR}}}{4\pi d^2 \langle v \rangle}, \quad (34)$$

where  $\langle v \rangle$  is the average CR velocity. For the fiducial values of  $p_{\text{CR}} = 0.1$  and  $E_{\text{SN}} = 10^{52} \text{ erg}$ , we obtain

$$U_{15} = \left\{ \begin{array}{l} 42 \\ 42 \\ 44 \\ 15 \end{array} \right\} \left( \frac{d}{10 \text{ kpc}} \right)^{-2} \left( \frac{\text{SFR}}{20 M_{\odot} \text{ yr}^{-1}} \right). \quad (35)$$

From equations (31) and (35),

$$J_{21} = \left\{ \begin{array}{l} 15 \\ 38 \\ 3.1 \times 10^2 \\ 1.4 \times 10^3 \end{array} \right\} U_{15}. \quad (36)$$

X-rays are mainly emitted by high-mass X-ray binaries. Observationally, the X-ray luminosities in 2–10 keV of local star-forming galaxies are related with their star formation rates as (e.g., Glover & Brand 2003)

$$L_{\text{X}} = 1.2 \times 10^{40} \left( \frac{\text{SFR}}{20 M_{\odot} \text{ yr}^{-1}} \right) \text{ erg s}^{-1}, \quad (37)$$

namely,

$$J_{\text{X},21} = 4.5 \times 10^{-3} \left( \frac{d}{10 \text{ kpc}} \right)^{-2} \left( \frac{\text{SFR}}{20 M_{\odot} \text{ yr}^{-1}} \right). \quad (38)$$

Although this is an empirical relation for local galaxies, observations of Lyman-break galaxies provide supports for this to be valid as far as  $z \sim 4$  (Glover & Brand 2003 and references therein). Here, we thus extend the relation (38) to high-redshift (say,  $z \sim 10$ ) universe. From equations (31) and (38), we obtain

$$J_{21} = \left\{ \begin{array}{l} 1.4 \times 10^5 \\ 3.5 \times 10^5 \\ 3.0 \times 10^6 \\ 3.7 \times 10^6 \end{array} \right\} J_{X,21}. \quad (39)$$

In Fig. 6 (a), we plot the relations (36) for the IMF cases (i)-(iv) in Table 2. The FUV intensity and CR energy density from galaxies are expected to fall on this relation. In the case of Pop II radiation sources (i.e., type i), which are characterized by  $T_* \sim 10^4$  K, the relation (36) intersects with the  $J_{\text{crit}}$  curve at  $(J_{21}, U_{15}) = (20, 2)$ , where the  $J_{\text{crit}}$  does not deviate yet from its no-CR value. This means that the CR ionization does not modify the value of  $J_{\text{crit}}$  significantly. On the other hand, for Pop III star clusters ( $T_* \sim 10^5$  K), the critical FUV flux at the intersection points are  $\gtrsim 20$  (type ii), 10 (iii), and 2 times (iv) as large as  $J_{\text{crit}}$  in the no-CR case, respectively. Namely, the CR ionization drastically changes the critical FUV flux except for the case with the top-heavy IMF with  $m_{\text{OB}} = 120 M_{\odot}$ .

In Fig. 6 (b), we also plot the relations (39) between  $J_{21}$  and  $J_{X,21}$ . As in the case of CRs, the X-ray ionization effects become important for higher  $T_*$ , in particular,  $T_* \gtrsim 10^4$  K.

## 6 CONCLUSION AND DISCUSSION

We have calculated the thermal evolution of primordial clouds under strong far-ultraviolet (FUV) fields, along with cosmic rays (CRs)/X-rays. In the cloud under a FUV field exceeding a threshold, the  $\text{H}_2$  cooling is suppressed at any density. Such a cloud collapses almost isothermally at 8000 K by hydrogen atomic cooling. According to numerical simulations (Bromm & Loeb 2003), it avoids fragmentation and collapses directly to a supermassive star (SMS).

Without external ionization by CRs/X-rays, the critical FUV flux is  $J_{\text{crit}} \simeq 1.6 \times 10^4$  (in units of  $10^{-21} \text{ erg s}^{-1} \text{ cm}^{-2} \text{ sr}^{-1} \text{ Hz}^{-1}$ ) for a diluted black body spectrum with brightness temperature  $T_* = 10^5$  K, while it is as small as  $J_{21} \simeq 20$  for  $T_* = 10^4$  K. This dependence on  $T_*$  comes from the higher  $\text{H}^-$  photodissociation ( $> 0.755$  eV) rate for lower  $T_*$  at the same  $J_{21}$  normalized at 13.6 eV. Since  $\text{H}_2$  is produced through the  $\text{H}^-$  channel (reactions 3 and 4 in Table 1), the larger  $\text{H}^-$  photodissociation reduces the amount of  $\text{H}_2$  and thus the value of  $J_{\text{crit}}$ .

We have studied how this critical FUV flux changes with simultaneous irradiation of either CRs or X-rays. In the case of CR irradiation, the critical FUV flux  $J_{\text{crit}}$  begins to increase with the CR energy density  $U_{\text{CR}} \gtrsim 10^{-14} \text{ erg cm}^{-3}$  and depends as  $J_{\text{crit}} \propto U_{\text{CR}}^{1/2}$  asymptotically. Similarly, for X-ray irradiation,  $J_{\text{crit}} \propto J_{\text{X}}^{1/2}$  for  $J_{\text{X}} \gtrsim 10^{-24} \text{ erg s}^{-1} \text{ cm}^{-2} \text{ sr}^{-1} \text{ Hz}^{-1}$  at 1 keV. In both cases, the increase of the critical FUV flux is caused by the enhanced ionization by CRs/X-rays, which promotes the  $\text{H}_2$  formation and cooling.

FUV intensity and CRs/X-rays from star-forming galaxies are expected to correlate each other since they all

trace the massive-star forming activity. Using the expected relations between FUV intensity and CRs/X-rays, we have found that if the initial mass function (IMF) of the radiation source is Salpeter-like and the brightness temperature of the FUV radiation is rather high  $T_* \sim 10^5$  K, the critical FUV intensity increases significantly  $J_{\text{crit}} \sim 10^6$  owing to ionization by CRs and X-rays. Even with the top-heavy IMF, the critical FUV intensity increases to  $J_{\text{crit}} \sim 10^5$  unless the stellar mass is  $\gtrsim 100 M_{\odot}$ . Since the fraction of halos exposed to FUV flux exceeding  $J_{\text{crit}}$  decreases exponentially with  $J_{\text{crit}}$  for  $\gtrsim 2 \times 10^3$  (Dijkstra et al. 2008), there is little possibility ( $\lesssim 10^{-28}$ ) for such intense FUV field realized in any halos. We conclude that if the radiation source is composed of Pop III stars with brightness temperature  $\sim 10^5$  K and contains sources of CRs/X-rays, its IMF must be very top-heavy  $\gtrsim 100 M_{\odot}$  to enable SMS formation in nearby halos. Other possible radiation sources enabling SMS formation include, e.g., sources with low brightness temperature,  $T_* \simeq 10^4$  K, such as Pop II/I star clusters, or those with high  $T_*$  but without strong CRs and X-rays. The latter possibility is realized if a Pop III star cluster is so young that it harbors neither supernova remnants nor high-mass X-ray binaries.

We have also found that the extragalactic ionization effects (CRs/X-rays) are able to promote the HD formation and cooling even if the clouds are irradiated with FUV radiation. Without external ionization, Yoshida et al. (2007) and Wolcott-Green & Haiman (2011) showed that the HD formation is suppressed by FUV radiation with  $J_{21} \gtrsim 10^{-2}$  for  $T_* = 10^4$  K, and that the number of metal-free stars ( $\gtrsim 10 M_{\odot}$ ) formed in HII regions by HD cooling (so-called Population III.2 stars) is reduced. However, we find the possibility that such stars can form under FUV radiation if strong CRs/X-rays ionize the clouds. These mean that the star formation in HII regions by HD cooling is not suppressed so strongly as previous thought (see also Wolcott-Green & Haiman 2011).

Finally, we discuss limitations of our analysis. We have treated the cloud evolution at the center by the one-zone model, where two assumptions have been made. First one is that the density increases approximately at the free-fall rate (equation 1). This is a good approximation for the isothermal spherically symmetric collapse. In reality, however, in addition to the thermal pressure, the turbulent support and compression, as well as the centrifugal support, which we have not taken into account, can have importance in dynamics, which controls the collapse rate. For example, in relatively massive halos, which we have considered here, the primordial gas is known to be in a state of turbulence (Wise & Abel 2007; Greif et al. 2008). Such turbulence might affect the thermal evolution, as well as the exact value of the FUV critical intensity for suppressing  $\text{H}_2$  cooling. If the angular momentum is present, the centrifugal force becomes more important with contraction relative to the gravity, and eventually halts the collapse. We here, however, only considered a rather low-density regime, and thus the angular momentum effect is not so dynamically important in our case. Another assumption in our model is that the external radiation is attenuated with the column density estimated by the central density and the size of the core, which is given by the Jeans length (equation 7). Although the column density of the core is given by this value for the Larson-Penston solu-

tion, the contribution from the envelope needs to be added. But we can see the envelope contribution is not significant by the following consideration. The steep decline of density with radius as  $\rho \propto r^{-2}$  limits the column density of hydrogen nuclei  $N_{\text{H}}$  in the envelope at most that of the core. Due to the photodissociation and low formation rate, the  $\text{H}_2$  abundance is remarkably lower in the envelope than in the core. Therefore, the envelope contribution to the column density of  $\text{H}_2$ , which is relevant for evaluating the critical FUV intensity, is small and the  $\text{H}_2$  column density is well approximated by that of the core. Another concern is about the geometry of the cloud. In the low-density regime we considered, the cloud shape can strongly deviate from the sphere. Even though the clouds are in such shapes as sheet-like or filamentary, however, the length scale of the shortest axis, which is most relevant for the shielding effects, is still roughly given by the Jeans length, and thus the our assumption of the Jeans length shielding remains valid. In fact, Shang et al. (2010), who studied the evolution of the primordial clouds under strong FUV irradiation and compared the results by the one-zone model and those by the cosmological three-dimensional simulation, found very good agreements as for the thermal evolution at the center of the clouds, as well as for the critical FUV intensity  $J_{\text{crit}}$  needed to quench the  $\text{H}_2$  formation/cooling. In addition, we assume that the clouds are isotropically irradiated by FUV, as well as CRs and X-rays. However, such intense FUV field as exceeding the critical value  $J_{\text{crit}}$  tends to be dominated by a nearby single large source, rather than by a collective effect of a large number of sources (Dijkstra et al. 2008). We suspect that, in the case of such anisotropic radiation field, more intense sources are necessary to induce SMS formation as the radiation comes from only limited solid angles. To confirm it, however, detailed modeling is required, which is beyond the scope of this paper.

## ACKNOWLEDGMENTS

We would like to thank Takashi Nakamura for his continuous encouragement, and Takashi Hosokawa and Susumu Inoue for fruitful discussions. This work is supported by the Grant-in-Aid for the Global COE Program "The Next Generation of Physics, Spun from Universality and Emergence" from the Ministry of Education, Culture, Sports, Science and Technology (MEXT) of Japan. K.I. is supported by the Grants-in-Aid for the Japan Society for the Promotion of Science Fellows (23-838). K.O. is supported by the Grants-in-Aid by the Ministry of Education, Science and Culture of Japan (19047004, 2168407, and 21244021).

## REFERENCES

Abel, T., Anninos, P., Zhang, Y., & Norman, M. L. 1997, *New Astron*, 2, 181  
 Alvarez, M. A., Wise, J. H., & Abel, T. 2009, *ApJL*, 701, L133  
 Bell, A. R. 1978, *MNRAS*, 182, 147  
 Bromm, V., & Loeb, A. 2003, *ApJ*, 596, 34  
 Campanelli, M., Lousto, C. O., Zlochower, Y., & Merritt, D. 2007, *Physical Review Letters*, 98, 231

Chandrasekhar, S. 1964a, *Physical Review Letters*, 12, 114  
 Chandrasekhar, S. 1964b, *ApJ*, 140, 417  
 Dijkstra, M., Haiman, Z., Mesinger, A., & Wyithe, J. S. B. 2008, *MNRAS*, 391, 1961  
 Fan, X. 2006, *New Astron Rev.*, 50, 665  
 Ferland, G. J., Peterson, B. M., Horne, K., Welsh, W. F., & Nahar, S. N. 1992, *ApJ*, 387, 95  
 Galli, D., & Palla, F. 1998, *A&A*, 335, 403  
 Galli, D., & Palla, F. 2002, *Planet. Space Sci.*, 50, 1197  
 Glover, S. C. O., & Brand, P. W. J. L. 2003, *MNRAS*, 340, 210  
 Greif, T. H., Johnson, J. L., Klessen, R. S., & Bromm, V. 2008, *MNRAS*, 387, 1021  
 Haiman, Z., & Loeb, A. 2001, *ApJ*, 552, 459  
 Haiman, Z., Rees, M. J., & Loeb, A. 1996, *ApJ*, 467, 522  
 Haiman, Z., Rees, M. J., & Loeb, A. 1997, *ApJ*, 476, 458  
 Hayakawa, S., Nishimura, S., & Takayanagi, T. 1961, *PASJ*, 13, 184  
 Herrmann, F., Hinder, I., Shoemaker, D., Laguna, P., & Matzner, R. A. 2007, *ApJ*, 661, 430  
 Indriolo, N., Geballe, T. R., Oka, T., & McCall, B. J. 2007, *ApJ*, 671, 1736  
 John, T. L. 1988, *A&A*, 193, 189  
 Koppitz, M., Pollney, D., Reisswig, C., Rezzolla, L., Thornburg, J., Diener, P., & Schnetter, E. 2007, *Physical Review Letters*, 99, 041102  
 Larson, R. B. 1969, *MNRAS*, 145, 271  
 Li, Y., et al. 2007, *ApJ*, 665, 187  
 Martin, P. G., Schwarz, D. H., & Mandy, M. E. 1996, *ApJ*, 461, 265  
 McCall, B. J., et al. 2003, *Nature*, 422, 500  
 Milosavljević, M., Couch, S. M., & Bromm, V. 2009, *ApJL*, 696, L146  
 Nakamura, F., & Umemura, M. 2002, *ApJ*, 569, 549  
 Omukai, K. 2001, *ApJ*, 546, 635  
 Omukai, K., Schneider, R., & Haiman, Z. 2008, *ApJ*, 686, 801  
 Palla, F., Salpeter, E. E., & Stahler, S. W. 1983, *ApJ*, 271, 632  
 Penston, M. V. 1969, *MNRAS*, 144, 425  
 Regan, J. A., & Haehnelt, M. G. 2009a, *MNRAS*, 393, 858  
 Regan, J. A., & Haehnelt, M. G. 2009b, *MNRAS*, 396, 343  
 Rybicki, G. B., & Lightman, A. P. 1979, *New York, Wiley-Interscience*, 1979. 393 p.,  
 Savin, D. W. 2002, *ApJ*, 566, 599  
 Schaerer, D. 2002, *A&A*, 382, 28  
 Schaerer, D. 2003, *A&A*, 397, 527  
 Schlickeiser, R. 2002, *Cosmic ray astrophysics / Reinhard Schlickeiser, Astronomy and Astrophysics Library; Physics and Astronomy Online Library*. Berlin: Springer. ISBN 3-540-66465-3, 2002, XV + 519 pp.,  
 Shang, C., Bryan, G. L., & Haiman, Z. 2010, *MNRAS*, 402, 1249  
 Shapiro, P. R., & Kang, H. 1987, *ApJ*, 318, 32  
 Shapiro, S. L., & Teukolsky, S. A. 1983, *Research supported by the National Science Foundation*. New York, Wiley-Interscience, 1983, 663 p.,  
 Shibata, M., & Shapiro, S. L. 2002, *ApJL*, 572, L39  
 Shull, J. M., & van Steenberg, M. E. 1985, *ApJ*, 298, 268  
 Spitzer, L., Jr., & Scott, E. H. 1969, *ApJ*, 158, 161  
 Spitzer, L., Jr., & Tomasko, M. G. 1968, *ApJ*, 152, 971  
 Stacy, A., & Bromm, V. 2007, *MNRAS*, 382, 229

- Stancil, P. C. 1994, *ApJ*, 430, 360  
Volonteri, M., Haardt, F., & Madau, P. 2003, *ApJ*, 582, 559  
Webber, W. R. 1998, *ApJ*, 506, 329  
Wolcott-Green, J., & Haiman, Z. 2011, *MNRAS*, 412, 2603  
Wolfire, M. G., Hollenbach, D., McKee, C. F., Tielens, A. G. G. M., & Bakes, E. L. O. 1995, *ApJ*, 443, 152  
Wise, J. H., & Abel, T. 2007, *ApJ*, 665, 899  
Yoshida, N., Omukai, K., Hernquist, L., & Abel, T. 2006, *ApJ*, 652, 6  
Yoshida, N., Omukai, K., & Hernquist, L. 2007, *ApJL*, 667, L117  
Zeldovich, Y. B., & Novikov, I. D. 1971, Chicago: University of Chicago Press, 1971,

This paper has been typeset from a  $\text{\TeX}$ / $\text{\LaTeX}$  file prepared by the author.